Earth and Planetary Science Letters 272 (2008) 429–436

Contents lists available at ScienceDirect

Earth and Planetary Science Letters

journal homepage: www.elsevier.com/locate/epsl

Compositional effect on the pressure derivatives of bulk modulus of silicate melts

Zhicheng Jing *, Shun-ichiro Karato

Department of Geology and Geophysics, Yale University, New Haven, CT 06520, USA

ARTICLE INFO

Article history:
Received 10 January 2008
Received in revised form 25 April 2008
Accepted 6 May 2008
Available online 22 May 2008

Editor: L. Stixrude

Keywords:
silicate melts
density
equation of state
pressure derivative of bulk modulus
composition
error propagation

ABSTRACT

Although the bulk moduli (K_{T0}) of silicate melts have a relatively narrow range of values, the pressure derivatives of the isothermal bulk modulus (K'_{T0}) can assume a broad range of values and have an important influence on the compositional dependence of the melt compressibility at high pressure. Based on the melt density data from sink/float experiments at high pressures in the literature, we calculate K'_{T0} using an isothermal equation of state (EOS) (e.g., Birch–Murnaghan EOS and Vinet EOS) with the previously determined values of room-pressure density (ρ_0) and room-pressure bulk modulus (K_{T0}). The results show that best estimates of K'_{T0} vary considerably from ~3 to ~7 for different compositions. K'_{T0} is nearly independent of Mg # (molar Mg/(Mg+Fe)), but decreases with SiO_2 content. Hydrous melts have anomalously small K'_{T0} leading to a high degree of compression at high pressures. For anhydrous melts, K'_{T0} is ~7 for peridotitic melts, ~6 for picritic melts, ~5 for komatiitic melts, and ~4 for basaltic melts.

1. Introduction

Melting of silicates in the deep interior of terrestrial planets has likely played an important role in the evolution and dynamics of the planets. Examples of deep melting include the deep magma oceans during the early accretion processes of the planets (Ohtani, 1985; Agee and Walker, 1988a), the dehydration-induced melt layer above the 410-km boundary proposed by Bercovici and Karato (2003) and possibly evidenced by seismological observations (e.g., Revenaugh and Sipkin, 1994; Song et al., 2004), and the partial melts at the bottom of the lower mantle suggested by the ultra-low velocity zone in the D'' layer (Williams and Garnero, 1996; Stixrude and Karki, 2005). Equation of state (EOS) for silicate melts is critical to understand the processes of separation and migration of these deep melts, and hence to explore the geophysical and geochemical consequences of deep melting.

Deep melts may have a broad range of compositions. Effect of melt composition on density in the low pressure regime has been very well described by the ideal mixing model (e.g., Bottinga and Weill, 1970; Lange and Carmichael, 1987; Lange, 1997). However, this type of model cannot be directly extrapolated to high pressures because melts are highly compressible and the exact nature of compression at high pressures is not well known.

A common approach to study the density of materials at high pressures is to use an isothermal EOS such as the widely used Birch–Murnaghan EOS and the Vinet EOS. This type of EOS can be parameterized using the room-pressure density (ρ_0), room-pressure bulk modulus (K_{T0}), and the pressure derivatives of the bulk modulus at room pressure (K'_{T0}, K''_{T0}, …). For the pressure range relevant to the Earth's mantle, higher order parameters (K''_{T0}, …) are often truncated leaving ρ_0, K_{T0} and K'_{T0} as fitting parameters. Among them ρ_0 and K_{T0} are well constrained by room-pressure measurements. The compositional dependence of ρ_0 is successfully characterized by the ideal mixing model (e.g., Bottinga and Weill, 1970; Lange and Carmichael, 1987; Lange, 1997), and K_{T0} is relatively insensitive to composition except for alkaline elements (Rivers and Carmichael, 1987). Consequently, in most of mafic or ultramafic melts, the key parameters that control their densities at high pressures are ρ_0 and K'_{T0}.

However, the compositional dependence of K'_{T0} has not been well documented. Using a melting-curve analysis, Lange (2003, 2007) proposed an inverse relationship between K'_{T0} and K_{T0} at pressures less than 6 GPa. However, no explicit compositional dependence of K'_{T0} at high pressures (>6 GPa) was well resolved by this approach. Rigden et al. (1988, 1989) predicted that K'_{T0} is higher for melts with lower SiO_2 and Al_2O_3 contents based on the shock-wave studies of anorthite (An), diopside (DI), and An_{36}–Di_{64}. Recently Ai and Lange (2008) revised the results of Rigden et al. (1989) and confirmed that K'_{T0} decreases with increasing Al_2O_3 content. However such compositional dependence has not been confirmed for a broader range of compositions other than the An–Di system and komatiite. K'_{T0} was also constrained by melt density data at high pressures obtained from sink/float experiments (e.g., Agee, 1998; Ohtani and Maeda, 2001). However, most results of K'_{T0} in these studies were obtained by the

* Corresponding author. Tel.: +1 203 432 5791; fax: +1 203 432 3134.
E-mail address: zhicheng.jing@yale.edu (Z. Jing).

0012-821X/$ – see front matter © 2008 Elsevier B.V. All rights reserved.
doi:10.1016/j.epsl.2008.05.013

fitting method in which all of the three parameters (ρ_0, K_{T0}, K'_{T0}) or both K_{T0} and K'_{T0} are estimated by fitting the data to an equation of state. As we will show, such an approach is subject to large uncertainties in the estimated value of K'_{T0} because of a strong trade-off among various inferred parameters.

In this study, a different approach is applied to fit the isothermal EOS, which can significantly reduce the uncertainties in K'_{T0}. We then investigate the compositional dependence of K'_{T0} and discuss its influence on the melt density under deep mantle conditions.

2. Methods for the estimation of K'_{T0} and its uncertainties

2.1. Some notes on the methods for estimation of K'_{T0}

The density of materials as a function of pressure, temperature, and composition can be given by an isothermal EOS,

$$\rho(P,T,X)=\rho(P;\rho_0(T,X),K_{T0}(T,X),K'_{T0}(T,X),\cdots) \tag{1}$$

where the room-pressure density (ρ_0), the room-pressure bulk modulus (K_{T0}), and the pressure derivatives of bulk modulus at room pressure (K'_{T0}, K''_{T0}, …) are temperature and compositional dependent parameters. Two isothermal equations of state are widely used: the Birch–Murnaghan EOS and the Vinet EOS. We will mainly use the Birch–Murnaghan EOS as an example of an isothermal EOS, but all the methods can be easily adapted to other isothermal equations of state such as the Vinet EOS. For the pressure range in the Earth's mantle, the Birch–Murnaghan EOS is often truncated to the third order, which is given by Birch (1947)

$$P=\frac{3}{2}K_{T0}\left[\left(\frac{\rho}{\rho_0}\right)^{7/3}-\left(\frac{\rho}{\rho_0}\right)^{5/3}\right]\left\{1+\frac{3}{4}(K'_{T0}-4)\left[\left(\frac{\rho}{\rho_0}\right)^{2/3}-1\right]\right\} \tag{2}$$

with ρ_0, K_{T0}, and K'_{T0} are the parameters that depend on composition. These parameters can be constrained by fitting the EOS to the melt density data determined by isothermal compression experiments. However, melt density data at high pressures are so limited that a direct fitting to the density–pressure curve cannot give all the parameters at the same time with reasonable uncertainties. This requires additional constraints from other independent measurements.

The compositional dependence of ρ_0 as well as its temperature dependence can be calculated using the ideal mixing model (e.g., Lange and Carmichael, 1987; Lange, 1997; Ochs and Lange, 1997) in which the molar volume of a silicate melt is given by a linear combination of partial molar volumes of oxide components,

$$V=\sum_i X_i\overline{V}_i \tag{3}$$

where X_i and $\overline{V}_i$ are the molar fraction and the molar volume of the ith component. To a first-order approximation, the temperature dependence can be incorporated as

$$V=\sum_i X_i\left[\overline{V}_i+\frac{\partial\overline{V}_i}{\partial T}(T-T_{\mathrm{ref}})\right] \tag{4}$$

where $\frac{\partial\overline{V}_i}{\partial T}$ is the partial molar expansivity of the ith component and T_{ref} is the reference temperature. Then the room-pressure density at temperature T can be given by

$$\rho_0(T,X)=\frac{V}{\sum_i X_i M_i} \tag{5}$$

where M_i is the gram formula weight of the ith component. The partial molar quantities $\overline{V}_i$ and $\frac{\partial\overline{V}_i}{\partial T}$ have been calibrated by many studies. In this study we use the results of Lange (1997) for melt components other than FeO and H_2O. For FeO component the result from Lange and Carmichael (1987) is used, and for H_2O the result from Ochs and Lange (1997) is used. Results of ρ_0 for the melt compositions in this study are listed in Table 1.

In contrast to previous studies, we also calculate K_{T0} using the ideal mixing model of compressibility,

$$\frac{\partial V}{\partial P}=\sum_i X_i\left[\frac{\partial\overline{V}_i}{\partial P}+\frac{\partial^2\overline{V}_i}{\partial T\partial P}(T-T_{\mathrm{ref}})\right] \tag{6}$$

Then K_{T0} is given by

$$K_{T0}=-\left(V\frac{\partial P}{\partial V}\right)_0 \tag{7}$$

For components other than H_2O, $\frac{\partial\overline{V}_i}{\partial P}$ and $\frac{\partial^2\overline{V}_i}{\partial T\partial P}$ are given by the results of Kress and Carmichael (1991), which are based on ultrasonic sound velocity studies of silicate melts (e.g., Rivers and Carmichael, 1987; Kress and Carmichael, 1991). For the H_2O component, results based on density estimation at elevated pressure from Ochs and Lange (1997) are used. Results of calculated K_{T0} are also listed in Table 1.

There are some other calibrations for the partial molar quantities in the ideal mixing model in addition to the results mentioned above. An updated calibration is given by the study of Ghiorso and Kress (2004), in which they included many recent experimental data on both melt density and sound velocity, although data for hydrous melts were not included. We will compare the calculated results based on different calibrations in the Discussion section, and choose the above calibrations to make the presentation clear.

Consequently, K'_{T0} is the only parameter to be determined by using density data at high pressures. This type of approach was previously applied to silicate solids by Bass et al. (1981), where the static compression data were combined with ultrasonic studies to constrain K'_{T0} for several solid silicates. By a detailed error analysis, they showed that the uncertainties in K'_{T0} given by this method were significantly reduced. For silicate melts, this approach was once applied to the MORB composition by Agee (1998), however, values of K'_{T0} for the other melts in Agee (1998) were not constrained by the same approach.

This approach is better demonstrated by a normalized EOS. If we define the normalized density and pressure as

$$\rho^*=\rho(T,P,X)/\rho_0(T,X) \tag{8}$$

$$P^*=P/K_{T0}(T,X) \tag{9}$$

then, the normalized Birch–Murnaghan EOS is given by

$$P^*=\frac{3}{2}\left[(\rho^*)^{7/3}-(\rho^*)^{5/3}\right]\left\{1+\frac{3}{4}(K'_{T0}-4)\left[(\rho^*)^{2/3}-1\right]\right\} \tag{10}$$

where K'_{T0} is the only fitting parameter left in this equation. We note that the shape of a normalized EOS solely depends on the values of K'_{T0}. After calculating the normalized density and pressure, K'_{T0} is then obtained for each composition and temperature condition by solving Eq. (10).

2.2. Uncertainties in K'_{T0}

The uncertainties in K'_{T0} determined by this approach can be analyzed by the propagation of errors through the normalized density and pressure. We follow the approach described in Bass et al. (1981) and Angel (2000). We only summarize the results of error propagation here. The detailed analysis is presented in Appendix A.

There are mainly four error sources that can contribute to the uncertainties in K'_{T0}: the uncertainties in pressure (P), room-pressure density (ρ_0), room-pressure bulk modulus (K_{T0}), and high-pressure density (ρ). The uncertainties in pressure for the ex-situ high-pressure experiments come from the uncertainties in the pressure calibrations as well as the imperfect reproducibility in the experiments and may vary from lab to lab. A rough estimation of the relative uncertainty

Table 1
Compilation of experimental data and EOS parameters

	Peridotitic							Picritic	Komatiitic		Basaltic			Hydrous basaltic		Hydrous ultramafic			
	KLB-1[a]	IT8720[b]	MA[b]	MA[b]	PHN1611[c]	PHN1611[c]	Pyrolite[c]	Picritic[d]	Komatiite[a]	Komatiite[a]	MORB[e]	MORB[d]	MORB[d]	MORB+ 2 wt.% H_2O[f]	MORB+ 8 wt.% H_2O[f]	s3-a[g]	s7-a[g]	s5-a[g]	s6-a[g]
Composition (wt.%)																			
SiO_2	44.5	41.2	42.1	42.1	45.1	45.1	46.2	48.0	46.7	46.7	49.4	51.8	51.8	50.8	47.7	35.0	34.3	33.9	33.5
Al_2O_3	3.6	3.7	6.5	6.5	2.8	2.8	3.6	7.7	6.3	6.3	15.6	16.0	16.0	15.6	14.7	3.2	3.2	1.6	3.1
FeO	8.1	15.1	16.0	16.0	10.4	10.4	8.7	16.5	10.8	10.8	9.0	10.0	10.0	9.8	9.2	15.2	19.9	24.9	25.5
MgO	39.2	33.0	30.2	30.2	38.4	38.4	38.3	18.2	28.4	28.4	8.5	7.9	7.9	7.7	7.2	28.5	25.7	23.6	22.5
CaO	3.4	7.0	5.3	5.3	3.4	3.4	3.2	8.6	6.3	6.3	10.9	11.7	11.7	11.5	10.8	13.1	11.9	11.1	10.5
H_2O	–	–	–	–	–	–	–	–	–	–	–	–	–	2.0	8.0	5.0	5.0	5.0	5.0
Na_2O	–	–	–	–	–	–	–	–	–	–	3.1	2.7	2.7	2.7	2.5	–	–	–	–
Mg #	0.90	0.80	0.77	0.77	0.87	0.87	0.89	0.66	0.82	0.82	0.63	0.58	0.58	0.58	0.58	0.77	0.70	0.63	0.61
Experimental conditions and results																			
Pressure (GPa)	8.2	16.3	16	7.4	13.5	20.5	22.1	14.5	8.9	6	5.85	14.9	15.1	16.8	20.0	15.5	14.3	13.3	11.4
Temperature (K)	2273	2543	2603	2163	2303	2633	2633	2773	2173	2073	1673	2473	2773	2573	2473	2173	2173	2173	2173
ρ (g/cm^3)	3.21	3.56	3.56	3.31	3.42	3.59	3.6	3.49	3.37	3.19	3.23	3.52	3.50	3.55	3.58	3.551	3.542	3.533	3.518
EOS parameters																			
ρ_0 (g/cm^3)	2.643± 0.001	2.663± 0.023	2.649± 0.025	2.760± 0.015	2.656± 0.014	2.571± 0.019	2.550± 0.017	2.590± 0.029	2.668± 0.011	2.691± 0.010	2.633± 0.003	2.524± 0.012	2.483± 0.016	2.364± 0.012	1.970± 0.011	2.433± 0.014	2.470± 0.016	2.514± 0.020	2.516± 0.020
K_{T0} (GPa)	23.4±3.6	19.6±3.1	20.3±3.3	22.5±2.3	22.7±3.5	20.8±4.3	21.6±4.5	20.9±2.8	22.9±2.2	23.1±1.9	18.8±0.3	20.8±1.4	21.6±2.1	18.2±1.2	14.5±0.8	17.8±1.3	17.3±1.2	16.9±1.1	16.7±1.1
K_{T0}'(B-M)	6.2±2.2	7.8±1.9	6.9±1.7	6.7±12.0	7.0±1.9	6.7±1.8	6.5±1.7	5.7±1.3	4.3±1.1	4.9±1.6	4.1±0.8	4.6±0.6	4.1±0.7	4.0±0.4	3.2±0.2	4.4±0.5	4.6±0.6	4.9±0.7	4.2±0.6
K_{T0}'(Vinet)	6.2	7.6	6.9	6.7	7.0	6.8	6.6	5.9	4.5	5.1	4.3	4.8	4.3	4.2	3.0	4.6	4.8	5.2	4.4

[a] Agee and Walker (1993).
[b] Suzuki et al. (1998).
[c] Suzuki and Ohtani (2003).
[d] Ohtani and Maeda (2001).
[e] Agee (1998).
[f] Sakamaki et al. (2006).
[g] Matsukage et al. (2005).

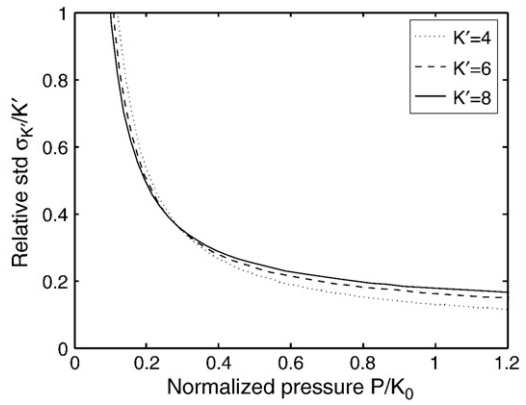

Fig. 1. Relative uncertainty (one standard deviation) in K'_{T0} as a function of pressure at which the melt density is determined. Solid curve, dashed curve, and the dotted curve are for K'_{T0}=4, 6, and 8, respectively. The uncertain is much smaller when K'_{T0} is obtained from a density data point at high pressure. Therefore only density data at pressures higher than 6 GPa (about 0.3 in terms of the normalized pressure) are used. These data can give an uncertainty of 15–30%.

(defined as $\frac{\sigma_P}{P}$, where σ_P is the standard deviation of P) would be around 5% (corresponds to a deviation of 0.5 GPa at 10 GPa (e.g., Matsukage et al., 2005; Sakamaki et al., 2006). The relative uncertainties in ρ determined from sink/float method are estimated to be about 1% (e.g., Matsukage et al., 2005; Sakamaki et al., 2006). The uncertainties in calculating ρ_0 and K_{T0} can be obtained by propagating the errors in the calibrated partial molar quantities, which were given in the aforementioned literature. For each melt composition, these uncertainties are calculated and listed in Table 1. The uncertainties in ρ_0 are in the range of 0.1–1.1%; the uncertainties in K_{T0} are in the range of 1% to 21%. In general, when an extrapolation to a higher temperature is needed, the uncertainties are larger. These propagated uncertainties are consistent with the reported average uncertainties: 0.4% for ρ_0 of the FeO-bearing dry silicate melts (Lange, 1994), and about 0.6% for hydrous melts (Ochs and Lange, 1997, 1999). For K_{T0}, the average uncertainties are estimated to be about 4% in Lange and Carmichael (1987) (uncertainties should be smaller for Kress and Carmichael (1991), which is used in this study, due to the better treatment of the oxidation states of iron in the melts) for dry melts. However, the extrapolation to high temperatures gives relatively large uncertainties since the temperature dependence of K_{T0} is poorly constrained.

Based on the formulation of error propagation derived in Appendix A, the uncertainties in K'_{T0} can be estimated given the above error sources. Fig. 1 shows the relative uncertainties in K'_{T0} for fitting a hypothetical data point at various pressures to the Birch–Murnaghan EOS, assuming constant input errors in P, ρ, ρ_0, and K_{T0} are 5%, 1%, 1%, and 10%. This diagram shows that given fixed relative uncertainties in all error sources, a fitting to a data point at relatively high pressures can give a smaller uncertainty in K'_{T0} than the fitting to a data point at low pressures. This is because the data point at high pressure provides a larger pressure span so that the pressure derivatives are better constrained. Therefore for the purpose of this paper we prefer to use sink/float data determined at pressures higher than 6 GPa, which give a relative uncertainty in K'_{T0} around 15–30%.

3. Data set

As mentioned in the previous section, melt density data at high pressures are used to constrain K'_{T0}. In this study, all melt density data are from sink/float experiments. These include Agee and Walker (1988b, 1993), Suzuki et al. (1995), Agee (1998), Suzuki et al. (1998), Ohtani and Maeda (2001), and Suzuki and Ohtani (2003) for dry melt compositions and Matsukage et al. (2005) and Sakamaki et al. (2006) for hydrous melt compositions. In sink/float experiments, the melt density can be bracketed by those of the density markers sinking or floating in each experiment. The experimental data used in this study are listed in Table 1. The experimental conditions fall in a temperature range of 1673 K–2773 K and a pressure range of 6–22 GPa. The melt compositions vary from peridotites to komatiites and to basalts; from anhydrous melts to hydrous melts. The Mg # (defined as molar ratio Mg/(Mg+Fe)) varies from 0.6 to 0.9. SiO_2 content is from 41 wt.% to 52 wt.% (or 37 mol% to 54 mol%) for dry melts. H_2O content is 5 wt.% in the hydrous ultramafic melts studied in Matsukage et al. (2005) and either 2 wt.% or 8 wt.% in hydrous MORB studied in Sakamaki et al. (2006).

This data set includes most available melt density data from sink/float methods. However, there are a few exceptions. The data for fayalite composition of Agee (1992) are not included due to the low pressure conditions and possible complication of the oxidation state of Fe component. The results of Smith and Agee (1997) for a picritic melt are not included because these data were obtained at relatively low pressure conditions (less than 5 GPa), which result in larger uncertainties in K'_{T0} when using our method (see Fig. 1). Data from Circone and Agee (1996) are not used because the melt contains a significant amount of TiO_2, which is not the focus of our current study.

4. Results

All the melt density data we have compiled are analyzed by the fitting method described in the Methods section. Results of fitted values and uncertainties of K'_{T0} for the whole data set are calculated and listed in Table 1. Contrary to silicate solids, whose K'_{T0} fall in a relatively small range of 4–6, K'_{T0} varies from 3 to 7 for the melt compositions studied here. The relative uncertainties in K'_{T0} are within 7–40% (mostly around 15–30%) for these melts, and the absolute uncertainties fall in the range of 0.2–2.2. Given these results, we can study the compositional effect on K'_{T0}.

4.1. Effect of temperature on K'_{T0}

As discussed in the Methods section, K'_{T0} is a function of temperature and composition in the isothermal EOS. To study the compositional effect on K'_{T0}, temperature effect must be examined first. However, for the temperature variation in the Earth's mantle, which is about 400–500 K across the depth range of 1000 km, the temperature effect is likely very small. This is illustrated in Fig. 2, where we plot the fitted values of K'_{T0} for a few melt compositions at different temperatures: MA at 2163 K and 2603 K, PHN1611 at 2303 K and 2633 K, MORB 2473 K and 2773 K, and komatiite at 2073 K and 2173 K. The differences in K'_{T0} at different temperatures are less than 0.5, which is smaller than the uncertainties in K'_{T0}. On the contrary, the

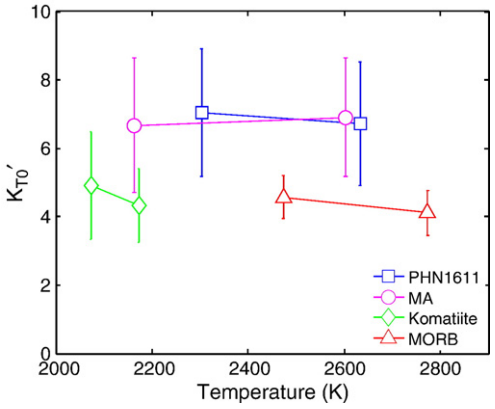

Fig. 2. Temperature effect on K'_{T0}. Results of K'_{T0} for melt composition PHN1611, MA, komatiite, and MORB at different temperatures are shown by the squares, circles, diamonds, and triangles, respectively. Error bars show one standard deviation in K'_{T0}. This figure shows that temperature has a negligible effect on K'_{T0}.

difference in K'_{T0} due to different compositions could be as large as 3, which is distinguishably larger than the uncertainties in K'_{T0}. This means that the temperature effect is negligible compared to the compositional effect. Therefore, we will neglect the temperature effect on K'_{T0} hereafter and directly compare the results of K'_{T0} at different temperatures without any corrections.

4.2. Effect of FeO, MgO and SiO_2

Deep melts could have a wide range of components, which makes the study of compositional effect complicated. However, unlike transport properties, which may highly depend on the behavior of a trace amount of minor components, density of silicate melts is mainly determined by major components like SiO_2, Al_2O_3, FeO, MgO, CaO, and maybe in some cases H_2O. Other components like Na_2O, K_2O, CO_2 are less important (although could be important when their amounts are large), and will not be discussed in this paper. Among these components, SiO_2, FeO, and MgO are the most interesting components due to their high abundances in deep mantle melts. Besides there are other reasons which make these components important: FeO component has a much higher "density" (defined by the ratio of molar mass to partial molar volume) than other components so additional FeO can significantly increase melt density as shown by Matsukage et al. (2005); Although SiO_2 is not particularly dense or light compared to other components, it may have a very distinct compression behavior due to its ability to change coordination (e.g., Stixrude and Karki, 2005). We will also discuss some effect of water, which is important due to its very small "density" and highly compressible nature compared to other components.

We plot the results of K'_{T0} for all the peridotitic melts as a function of Mg # in Fig. 3a. There is only a small difference in SiO_2 content for these peridotites (see Table 1). However, the difference in FeO/MgO content is relatively large. The Mg # ranges from 0.77 to 0.90. The results show that K'_{T0} is nearly independent of Mg #. Similar results for hydrous ultramafic melt compositions are also shown in Fig. 3a, in which case K'_{T0} does not vary with the Mg # when the SiO_2, H_2O, and Al_2O_3 contents remain nearly the same.

Unlike the dependence on the composition of divalent cations, K'_{T0} has a strong dependence on SiO_2 content, which is illustrated in Fig. 3b. K'_{T0} decreases from ~7 to ~4 for dry melts when SiO_2 content increases from 37 mol% to 54 mol%. That is, if we have more SiO_2 in a melt, the bulk modulus of the melts will not increase very fast with increasing pressure, which could make the melt relatively more compressible than the SiO_2-poor melt at high pressure. This observation confirms the similar prediction by Rigden et al. (1989), which was based on the results of An–Di system. Note that for natural melt compositions with higher SiO_2 content, the Al_2O_3 contents are also higher. For example, MORB has ~10 mol% Al_2O_3, while peridotites only have ~2 mol% Al_2O_3. Therefore it is important to separate the effects of SiO_2 and Al_2O_3. Ai and Lange (2008) conducted ultrasonic measurements for CaO–MgO–$Al2O_3$–SiO_2 melts and revised the values of K'_{T0} of Rigden et al. (1989). Their results show that K'_{T0} decreases from 6.8 to 4.7 when Al_2O_3 content increases from 0 to 25 mol%. If the effect of Al_2O_3 on decreasing K'_{T0} can be assumed universal for all silicate liquids that we have studied, then the effect of Al_2O_3 can be subtracted. This is shown in Fig. 3b., in which the dashed line shows the corrected effect of SiO2 on K'_{T0}. Therefore for the compositions in this study effect of SiO_2 on K'_{T0} is likely greater than that of Al_2O_3 due to the larger concentrations of SiO_2.

If this trend of K'_{T0} with SiO_2 content can be extrapolated to the SiO_2 end-member, then a very small K'_{T0} (~0 by extrapolating the dashed line in Fig. 3b.) would be obtained. This unusual behavior of the SiO_2 component seems to be supported by some other studies, although controversy still exists. Based on an experimental determination of partial molar volume of SiO_2 in silicate liquids at high pressures, Gaetani et al. (1998) obtained a very small K'_{T0} of ~−2 for the SiO_2 component in rhyolite liquid. Although a different calculation by Lange (2003) showed that K'_{T0} is ~10 for the SiO_2 component.

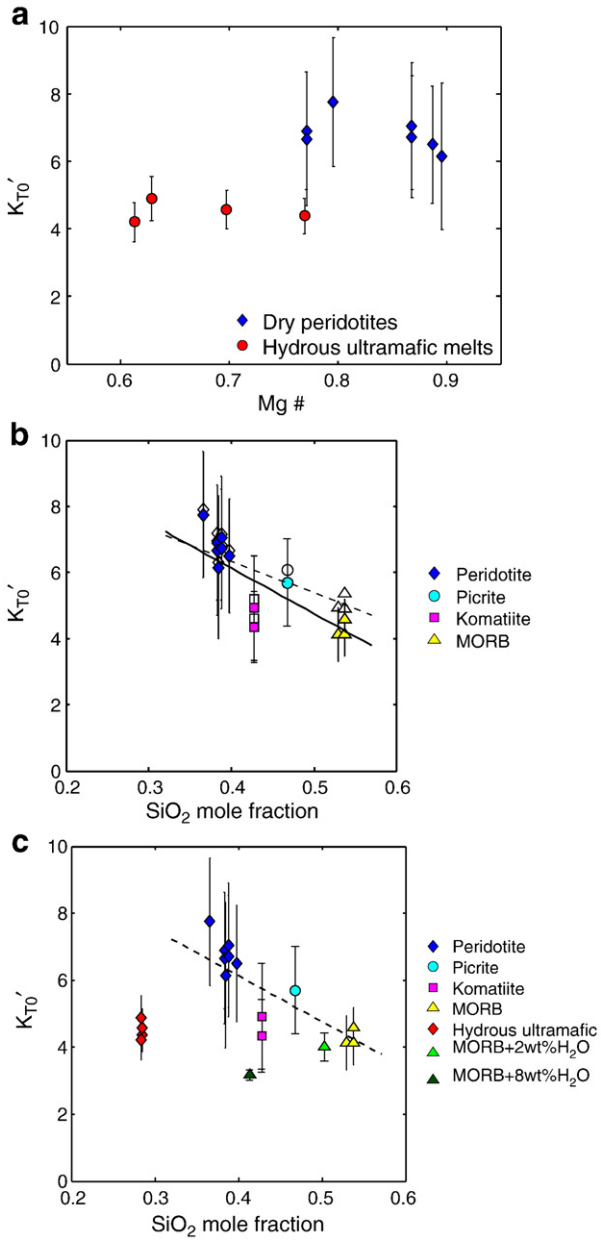

Fig. 3. Compositional effect on K'_{T0}: (a) effect of Mg # (molar ratio MgO/(MgO+FeO)); (b) effect of SiO_2. Empty symbols are the results of K'_{T0} with the effect of Al_2O_3 subtracted (see text). Solid and dashed lines are the weighted least square fit of data points without and with the correction for the effect of Al_2O_3. (c) effect of H_2O. Hydrous melts have smaller K'_{T0} than that of dry melts, which is roughly shown by the same dashed line as in (b).

Essentially, the small K'_{T0} of SiO_2-rich melts comes from the very efficient compression of the SiO_2 component. This can be explained by the continuous change of Si-coordination number from 4 to 6 with increasing pressure (e.g., Xue et al., 1989; Stixrude and Karki, 2005). As the coordination number increases, the continuing distortion of the Si–O–Si bond angle can significantly improve the packing efficiency of the melts (e.g., Rigden et al., 1989; also by the analogy with the great density difference of ~30% between coesite and stishovite). Therefore, the addition of SiO_2 component to a melt would increase the ability for compression at high pressure. Likewise, Al_2O_3 can also undergo a coordination change from 4 to 6, so a similar effect of Al_2O_3 on K'_{T0} is observed. There are other compression mechanisms that can also make SiO_2 component more compressible. These include the topological changes of ring structure in the silicate melts (Stixrude and Bukowinski, 1991).

Table 2
Fitted K'_{T0} for several melt compositions and comparison with other studies

References	Peridotite	Komatiite	MORB	Picrite	Hydrous melts
This study	6.8±0.7	4.5±0.9	4.3±0.4	5.7±1.3	4.5±0.3
Agee (1998)	5.9	4.25	4.4[a]	–	–
Ohtani and Maeda (2001)	6.2	–	5.0	7.6	–
Rigden et al. (1989)	–	–	4.85[b, c]	–	–
Miller et al. (1991)	–	4.9[c]	–	–	–

[a] Method used is similar to this study.
[b] A model basaltic composition with 36 mol% anorthite, and 64 mol% diopside.
[c] The difference between K'_{S0} and K'_{T0} is ignored.

4.3. Effect of H_2O

Effect of water on K'_{T0} is very significant. Results from hydrous ultramafic melts (Matsukage et al., 2005) and hydrous basaltic melts (Sakamaki et al., 2006) are shown in Fig. 3c. Even for melts with low SiO_2 content, K'_{T0} could still be very small if enough water is added to the system. This means that a hydrous melt is more compressible at high pressures than the corresponding dry melt. However, currently available data are only for a limited range of compositions and the details of the influence of water are not well constrained.

4.4. Results of K'_{T0} for some geologically important melts

According to the preceding analysis, SiO_2 content is the most important factor for the calculation of K'_{T0} whereas the Mg # of the melt is not as important. Consequently, it is reasonable to neglect the effect of Mg # and constrain the K'_{T0} only based on SiO_2 contents for several geologically interesting melts, including peridotites, picrites, komatiites, and basalts. Again the melt density data for dry melts in Table 1 are used. Dry melt compositions are divided into groups based on SiO_2 content. A weighted least-squares fitting to the normalized EOS (Eq. (10)) is used to obtain K'_{T0}. The results of K'_{T0} for different compositional groups are shown in Table 2. Fig. 4 shows compression curves with different K'_{T0}, which varies a lot from 4.3±0.4 for basaltic melts, to 4.5±0.9 for komatiitic melts, to 5.7±1.3 for picritic melts, and to 6.8±0.7 for peridotitic melts. The result for the hydrous ultramafic melts, which has a K'_{T0} around 4.5, is also shown in Fig. 4. Therefore, a basaltic melt is likely more compressible at high pressures than a peridotitic melt due to its higher SiO_2 content, that is, smaller K'_{T0}; and a hydrous ultramafic melt is likely more compressible at high pressure than a dry melt. However, much is unconstrained about the equation of state of hydrous melts. For example, we have only two different hydrous compositions: hydrous ultramafic melts from Matsukage et al. (2005) and hydrous MORB melts from Sakamaki et al. (2006), the influence of SiO_2 on K'_{T0} for hydrous melts was not investigated in this study.

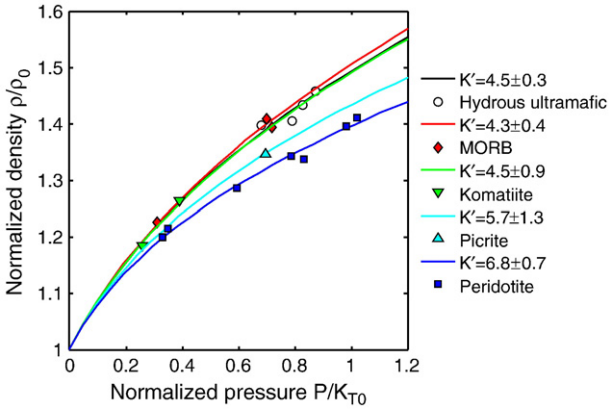

Fig. 4. Compression curves for some geologically interesting melts including peridotites, komatiites, picrites, MORB, and hydrous ultramafic melts. Density is normalized by the room-pressure density, and the pressure is normalized by the room-pressure bulk modulus. MORB and hydrous ultramafic melts have smaller K'_{T0}, which means that they are more compressible at high pressures.

5. Discussion

5.1. Uncertainty again

As we have demonstrated in the Methods section, room-pressure properties play a very important role in anchoring the EOS of silicate melts. Here we discuss the uncertainties due to different calibrations of ρ_0 and K_{T0}. Results of K'_{T0} calculated using different calibrations are compared in Fig. 5. Three different calculations are shown: (1) ρ_0 from Lange (1997) and K_{T0} from Kress and Carmichael (1991), which is same as in Fig. 3b; (2) ρ_0 from Lange (1997) and K_{T0} from Ghiorso and Kress (2004); (3) both ρ_0 and K_{T0} from Ghiorso and Kress (2004). Fig. 5 shows that all three calculations give similar although different results on K'_{T0} and the relationship between K'_{T0} and SiO_2 content remains the same. Consequently a different choice of calibrations would not change our conclusions on the composition dependence of K'_{T0}.

5.2. Comparison to other studies

K'_{T0} for a few geologically interesting melts are previously determined using sink/float data (Agee, 1998; Ohtani and Maeda, 2001). These results are compared to the results of this study in Table 2. Ohtani and Maeda (2001) determined K'_{T0} for MORB, picrite, and peridotite using similar data set of this study and obtained 5.0 for MORB, 6.2 for peridotite, and 7.6 for picrite. K'_{T0} for MORB and picrite are higher than the results of this study, but K'_{T0} for peridotite is lower. Also the trend in the compositional effect of SiO_2 on K'_{T0} is different than that of this study: peridotite has a smaller K'_{T0} than picrite. In the study of Agee (1998), K'_{T0} for three compositions including MORB, komatiite, and peridotite are determined. His result of K'_{T0}=4.25 for komatiite is similar to ours, but K'_{T0}=5.9 for peridotite is smaller. The differences between previous results and this study are largely due the difference in the fitting methods since similar experimental data were used in these studies. For most melt compositions in Agee (1998) and Ohtani and Maeda (2001) except for the MORB melt in Agee (1998), K_{T0} and K'_{T0} were constrained simultaneously by fitting to the isothermal EOS, which, as discussed in Bass et al. (1981) and this study, will lead to a trade-off between K_{T0} and K'_{T0}. In addition, when using sink/float results at different temperatures, the temperature effect on K_{T0} was simply neglected in Agee (1998) and Ohtani and

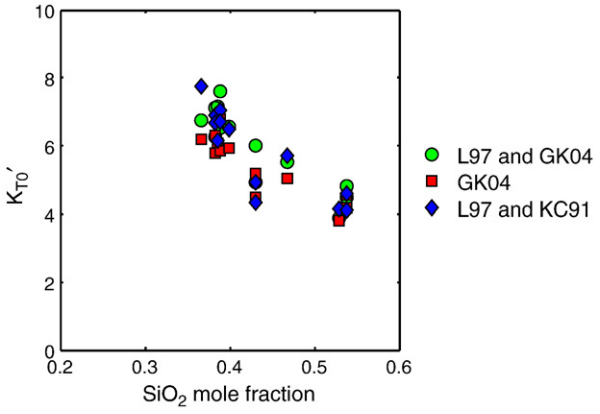

Fig. 5. Comparison of calculated results of K'_{T0} as a function of SiO_2 content using different room-pressure calibrations. Blue diamonds are the results using calibrations of ρ_0 from Lange (1997) and K_{T0} from Kress and Carmichael (1991), which is the same as in Fig. 3b; Green circles use calibrations of ρ_0 from Lange (1997) and K_{T0} from Ghiorso and Kress (2004); Red squares use the results of both ρ_0 and K_{T0} from Ghiorso and Kress (2004). (For interpretation of the references to color in this figure legend, the reader is referred to the web version of this article.)

Maeda (2001), although the temperature effect on density was corrected. As an exception, however, the result for MORB (K'_{T0}=4.4) in Agee (1998) is similar to our result because similar methods were applied.

K'_0 for komatiite and MORB are also determined from shock-wave measurements (Rigden et al., 1988; Miller et al., 1991) (Table 2), which give similar although slightly larger K'_0 than this study, if the difference between K'_{S0} and K'_{T0} is ignored (4.9 for komatiite compared to 4.5 in this study, and 4.85 for MORB compared to 4.3 in this study). Although in these studies the trade-off between K'_0 and K_0 still exists, larger data sets (6–13 data points) and wider pressure ranges than those of typical sink/float experiments can ensure much smaller uncertainties in K'_0.

5.3. Assumptions and limitations in this study

There are some limitations in our approach in the present study. (1) Using the third-order Birch–Murnaghan EOS for silicate melts is an assumption. We have also tested the Vinet EOS, which gives similar results in K'_{T0} (Table 1), and hence similar trends in the compositional dependences of K'_{T0}. (2) We assume that there is no phase transition in the silicate melts, i.e., no sharp change in the curvature of the compression curves, within the pressure range studied here. This has been verified for the An–Di system and komatiite by the shock-wave studies (Rigden et al., 1988, 1989; Miller et al., 1991), in which smooth compression curves were always observed. However, if there is indeed an abrupt change in the compression curve, then density data distributed over the whole pressure range are required to constrain the K'_{T0} for each smooth segment of the curve. (3) The calculation of K_{T0} by an ideal mixing model is an assumption. The physical picture of mixing is not clear for melts so there is no reason to believe that the ideal mixing model is better than other models. However, Rivers and Carmichael (1987) and Ai and Lange (2008) applied different ideal mixing models (mixing linearly with mole fraction or volume fraction of the components, or even the linear mixing in sound speed) to the ultrasonic data and found out that the compressibility of melts predicted from these models are nearly identical. This suggests that K_{T0} of silicate melts is likely insensitive to mixing models. (4) For the composition range of study only the effects MgO, FeO, SiO_2, and H_2O could be resolved. However, other melt components could have complex behaviors of compression. Therefore special caution must be taken when the relationship of K'_{T0} and SiO_2 content is extrapolated to the melt compositions which are very different from this study. For instance, a simple extrapolation may result in very small values of K'_{T0} for $KAlSi_3O_8$ and $NaAlSi_3O_8$ melts, whereas high values of K'_{T0} were shown by Lange (2003, 2007). (5) Finally we note that the data on hydrous melts are very sparse. Influence of water was studied only for a small range of water contents and of melt compositions.

5.4. Compositional effect on the density of silicate melts

In a summary, we have found that the most important melts components that control melt density at high pressures are FeO, SiO_2, and H_2O. FeO is a very dense component, which will increase ρ_0 of the melts considerably, but has no significant effects on K_{T0} and K'_{T0}. SiO_2 can slightly decrease ρ_0 and maybe K_{T0} depending on temperature, but will make melts more compressible at high pressures due to its effect on K'_{T0}. H_2O has large effects on all the EOS parameters (ρ_0, K_{T0}, and K'_{T0}). It will decrease melt density significantly at low pressure. At high pressure, this reduction in density is partly compensated by the effect of H_2O on K_{T0} and K'_{T0}.

6. Conclusions

The pressure derivatives of bulk modulus of silicate melts for a range of compositions are determined from high-pressure density data using room-pressure density and bulk modulus of the melts. This method provides us with more robust estimates of K'_{T0} compared to the estimates by previous authors. Results show that the pressure derivative of bulk modulus is independent of Mg #, but has a systematic trend with SiO_2 content. H_2O component can also reduce the pressure derivative of bulk modulus significantly. A basaltic melt is likely more compressible at high pressures than a peridotitic melt due to its higher SiO_2 content, that is, smaller K'_{T0}. Similarly a hydrous melt is likely more compressible at high pressures than the corresponding dry melt.

Acknowledgments

This work was supported by the National Science Foundation. We thank Mainak Mookherjee and Takaaki Kawazoe for various discussions.

Appendix A. Error analysis

The procedure of error analysis in this work is mainly adapted from the analysis by Bass et al. (1981), which is based on the least-squares method. The Birch–Murnaghan EOS (Eq. (10)) can be linearized as

$$P^* = Q + aR \tag{A1}$$

by defining

$$Q(\rho^*) = \frac{3}{2}\left[(\rho^*)^{\frac{7}{3}} - (\rho^*)^{\frac{5}{3}}\right] \tag{A2}$$

$$R\left(\rho^*\right) = \frac{9}{8}\left[\left(\rho^*\right)^{\frac{7}{3}} - \left(\rho^*\right)^{\frac{5}{3}}\right]\left[\left(\rho^*\right)^{\frac{2}{3}} - 1\right] = \frac{3}{4}Q\left[\left(\rho^*\right)^{\frac{2}{3}} - 1\right] \tag{A3}$$

and

$$a = \left(K'_{T0} - 4\right) \tag{A4}$$

where a is the parameter to fit. The weighted least-squares solution of a is given by

$$a = \frac{\sum \frac{R_i P_i^*}{\sigma_i^2} - \sum \frac{R_i Q_i}{\sigma_i^2}}{\sum \frac{R_i^2}{\sigma_i^2}} \tag{A5}$$

where subscript i represents the ith data point, and σ_i is the total uncertainty of data point i. The summation is over the number of data points at high pressures. After some manipulation, σ_i can be calculated by the propagation of errors from the error sources as

$$\sigma_i^2 = \frac{\sigma_{Pi}^2}{P_i^2}\left(P_i^*\right)^2 + \frac{\sigma_{K_{T0}}^2}{K_{T0}^2}\left(P_i^*\right)^2 + \frac{\sigma_{\rho i}^2}{\rho_i^2}\frac{K_{Ti}^2}{K_{T0}^2} + \frac{\sigma_{\rho_0}^2}{\rho_0^2}\frac{K_{Ti}^2}{K_{T0}^2} \tag{A6}$$

where based on the Eulerian finite strain theory (e.g., Anderson, 1995)

$$\frac{K_T}{K_{T0}} = \left(\rho^*\right)^{\frac{5}{3}}\left\{1 + \frac{1}{2}\left(1 - \left(\rho^*\right)\right)^{\frac{2}{3}}\left[5 - 3K'_{T0} - \frac{27}{4}\left(4 - K'_{T0}\right)\left(1 - \left(\rho^*\right)^{\frac{2}{3}}\right)\right]\right\} \tag{A7}$$

Therefore the uncertainty in K'_{T0} is

$$\sigma_{K'_{T0}}^2 = \sigma_a^2 = \sum \sigma_i^2 \left(\frac{\partial a}{\partial P_i^*}\right)^2 = \frac{1}{\sum \frac{R_i^2}{\sigma_i^2}} \tag{A8}$$

For the case with only one density data point at high pressure, the uncertainty in K'_{T0} is simply given by

$$\sigma_{K'_{T0}}^2 = \frac{1}{R^2}\left(\frac{\sigma_P^2}{P^2}\left(P^*\right)^2 + \frac{\sigma_{K_{T0}}^2}{K_{T0}^2}\left(P^*\right)^2 + \frac{\sigma_{\rho_i}^2}{\rho^2}\frac{K_T^2}{K_{T0}^2} + \frac{\sigma_{\rho_0}^2}{\rho_0^2}\frac{K_T^2}{K_{T0}^2}\right) \tag{A9}$$

References

Agee, C.B., 1992. Isothermal compression of molten Fe_2SiO_4. Geophys. Res. Lett. 19, 1169–1172.

Agee, C.B., 1998. Crystal-liquid density inversions in terrestrial and lunar magmas. Phys. Earth Planet. Ineter. 107, 63–74.
Agee, C.B., Walker, D., 1988a. Mass balance and phase density constraints on early differentiation of chondritic mantle. Earth Planet. Sci. Lett. 90, 144–156.
Agee, C.B., Walker, D., 1988b. Static compression and olivine flotation in ultrabasic silicate liquid. J. Geophys. Res. 93, 3437–3449.
Agee, C.B., Walker, D., 1993. Olivin flotation in mantle melt. Earth Planet. Sci. Lett. 114, 315–324.
Ai, Y., Lange, R.A., 2008. New acoustic velocity measurements on CaO–MgO–Al_2O_3–SiO_2 liquids: reevaluation of the volume and compressibility of $CaMgSi_2O_6$–$CaAl_2Si_2O_8$ liquids to 25 GPa. J. Geophys. Res. 113, B04203. doi:10.1029/2007JB005010.
Anderson, O.L., 1995. Equations of State of Solids for Geophysics and Ceramic Science. Oxford University Press, Oxford.
Angel, R.J., 2000. Equations of state, high-temperature and high-pressure crystal chemistry. Rev. Mineral. Geochem. 35–59.
Bass, J.D., Liebermann, R.C., Weidner, D.J., Finch, S.J., 1981. Elastic properties from acoustic and volume compression experiments. Phys. Earth Planet. Ineter. 25, 140–158.
Bercovici, D., Karato, S., 2003. Whole-mantle convection and the transition-zone water filter. Nature 425, 39–44.
Birch, F., 1947. Finite elastic strain of cubic crystals. Phys. Rev. 71, 809–824.
Bottinga, Y., Weill, D.F., 1970. Densities of liquid silicate systems calculated from partial molar volumes of oxide components. Am. J. Sci. 269, 169–182.
Circone, S., Agee, C.B., 1996. Compressibility of molten high-Ti mare glass: evidence for crystal-liquid density inversions in the lunar mantle. Geochim. Cosmochim. Acta 60, 2709–2720.
Gaetani, G.A., Asimow, P.D., Stolper, E.M., 1998. Determination of the partial molar volume of SiO2 in silicate liquids at elevated pressures and temperatures: a new experimental approach. Geochim. Cosmochim. Acta 62, 2499–2508.
Ghiorso, M.S., Kress, V.C., 2004. An equation of state fro silicate melts. II. Calibration of volumetric properties at 10^5 Pa. Am. J. Sci. 304, 679–751.
Kress, V.C., Carmichael, I.S.E., 1991. The compressibility of silicate liquids containing Fe_2O_3 and the effect of composition, temperature, oxygen fugacity and pressure on their redox states. Contrib. Mineral. Petrol. 108, 82–92.
Lange, R.A., 1994. The effect of H_2O, CO_2 and F on the density and viscosity of silicate melts. In: Carroll, M.R., Holloway, J.R. (Eds.), Volatiles in Magmas. . Reviews in Mineralogy. Mineralogical Society of America, Washington, D. C., pp. 331–369.
Lange, R.A., 1997. A revised model for the density and thermal expansivity of K_2O–Na_2O–CaO–MgO–Al_2O_3–SiO_2 liquids from 700 to 1900 K: extension to crustal magmatic temperatures. Contrib. Mineral. Petrol. 130, 1–11.
Lange, R.A., 2003. The fusion curve of albite revisited and the compressibility of $NaAlSi_3O_8$ liquid with pressure. Am. Mineral. 88, 109–120.
Lange, R.A., 2007. The density and compressibility of $KAlSi_3O_8$ liquid to 6.5 GPa. Am. Mineral. 92, 114–123.
Lange, R.A., Carmichael, I.S.E., 1987. Densities of Na_2O–K_2O–CaO–MgO–FeO–Fe_2O_3–$A1_2O_3$–TiO_2–SiO_2 liquids: new measurements and derived partial molar properties. Geochim. Cosmochim. Acta 51, 2931–2946.
Matsukage, K.N., Jing, Z., Karato, S., 2005. Density of hydrous silicate melt at the conditions of Earth's deep upper mantle. Nature 438, 488–491.
Miller, G.H., Stolper, E.M., Ahrens, T.J., 1991. The equation of state of a molten komatiite 1. Shock wave compression to 36 GPa. J. Geophys. Res. 96, 11831–11848.
Ochs, F.A., Lange, R.A., 1997. The partial molar volume, thermal expansivity, and compressibility of H_2O in $NaAlSi_3O_8$ liquid: new measurements and an internally consistent model. Contrib. Mineral. Petrol. 129, 155–165.
Ochs, F.A., Lange, R.A., 1999. The density of hydrous magmatic liquids. Science 283, 1314–1317.
Ohtani, E., 1985. The primodial terrestrial magma ocean and its implication for stratification of the mantle. Phys. Earth Planet. Ineter. 38, 70–80.
Ohtani, E., Maeda, M., 2001. Density of basaltic melt at high pressure and stability of the melt at the base of the lower mantle. Earth Planet. Sci. Lett. 193, 69–75.
Revenaugh, J., Sipkin, S.A., 1994. Seismic evidence for silicate melt atop the 410 km mantle discontinuity. Nature 369, 474–476.
Rigden, S.M., Ahrens, T.J., Stolper, E.M., 1988. Shock compression of molten silicate: results for a model basaltic composition. J. Geophys. Res. 93, 367–382.
Rigden, S.M., Ahrens, T.J., Stolper, E.M., 1989. High-pressure equation of state of molten anorthite and diopside. J. Geophys. Res. 94, 9508–9522.
Rivers, M.L., Carmichael, I.S.E., 1987. Ultrasonic studies of silicate melts. J. Geophys. Res. 92, 9247–9270.
Sakamaki, T., Suzuki, A., Ohtani, E., 2006. Stability of hydrous melt at the base of the Earth's upper mantle. Nature 439, 192–194.
Smith, J.R., Agee, C.B., 1997. Compressibility of molten “green glass” and crystal-liquid density crossovers in low-Ti lunar magma. Geochim. Cosmochim. Acta 61, 2139–2145.
Song, T.-R.A., Helmberger, D.V., Grand, S.P., 2004. Low-velocity zone atop the 410-km seismic discontinuity in the northwestern United States. Nature 427, 530–533.
Stixrude, L., Bukowinski, M.S.T., 1991. A novel topological compression mechanism in a covalent liquid. Science 250, 541–543.
Stixrude, L., Karki, B., 2005. Structure and freezing of $MgSiO_3$ liquid in Earth's lower mantle. Science 310, 297–299.
Suzuki, A., Ohtani, E., 2003. Density of peridotite melts at high pressure. Phys. Chem. Miner. 30, 449–456.
Suzuki, A., Ohtani, E., Kato, T., 1995. Flotation of diamond in mantle melt at high pressure. Science 269, 216–218.
Suzuki, A., Ohtani, E., Kato, T., 1998. Density and thermal expansion of a peridotite melt at high pressure. Phys. Earth Planet. Ineter. 107, 53–61.
Williams, Q., Garnero, E.J., 1996. Seismic evidence for partial melt at the base of Earth's mantle. Science 273, 1528–1530.
Xue, X., Stebbins, J.F., Kanzaki, M., Tronnes, R.G., 1989. Silicon coordination and speciation changes in a silicate liquid at high pressures. Science 245, 962–964.